Inorganic Chemistry

pubs.acs.org/IC Article

Antiferromagnetic Order and Spin-Canting Transition in the Corrugated Square Net Compound $Cu_3(TeO_4)(SO_4)\cdot H_2O$

Zhi-Cheng Wang,* Kulatheepan Thanabalasingam, Jan P. Scheifers, Alenna Streeter, Gregory T. McCandless, Jonathan Gaudet, Craig M. Brown, Carlo U. Segre, Julia Y. Chan, and Fazel Tafti*

Cite This: https://doi.org/10.1021/acs.inorgchem.1c01220 Read Online

ABSTRACT: Strongly correlated electrons in layered perovskite structures have been the birthplace of high-temperature superconductivity, spin liquids, and quantum criticality. Specifically, the cuprate materials with layered structures made of corner-sharing square-planar CuO_4 units have been intensely studied due to their Mott insulating ground state, which leads to high-temperature superconductivity upon doping. Identifying new compounds with similar lattice and electronic structures has become a challenge in solid-state chemistry. Here, we report the hydrothermal crystal growth of a new copper tellurite sulfate, $Cu_3(TeO_4)(SO_4)\cdot H_2O$, a promising alternative to layered perovskites. The orthorhombic phase (space group *Pnma*) is made of corrugated layers of corner-sharing CuO_4 square-planar units that are edge-shared with TeO_4 units. The layers are linked by slabs of corner-sharing CuO_4 and SO_4. Using both the bond valence sum analysis and magnetization data, we find purely Cu^{2+} ions within the layers but a mixed valence of Cu^{2+}/Cu^{+} between the layers. $Cu_3(TeO_4)(SO_4)\cdot H_2O$ undergoes an antiferromagnetic transition at T_N = 67 K marked by a peak in the magnetic susceptibility. Upon further cooling, a spin-canting transition occurs at T^* = 12 K, evidenced by a kink in the heat capacity. The spin-canting transition is explained on the basis of a J_1−J_2 model of magnetic interactions, which is consistent with the slightly different in-plane superexchange paths. We present $Cu_3(TeO_4)(SO_4)\cdot H_2O$ as a promising platform for the future doping and strain experiments that could tune the Mott insulating ground state into superconducting or spin liquid states.

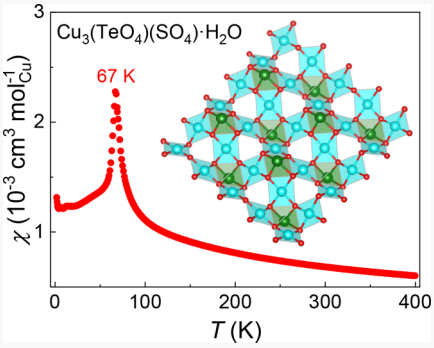

INTRODUCTION

Mott insulators are materials with half-filled bands, a nominally metallic configuration, but with strong correlations that lead to localized electronic states and insulating behavior. Such materials have been a focus of intense research, largely due to the discovery of high-T_c superconductivity in cuprate systems.[1] Aside from subtle structural differences, all cuprate superconductors have a layered crystal structure made of square networks of Cu−O−Cu bonds as illustrated in Figure 1a. Each Cu^{2+} with a single hole in the $d_{x^2-y^2}$ orbital acts as a spin-1/2 ion whose strong interaction with the neighboring ions leads to an antiferromagnetic (AFM) insulating ground state.[2] Since all bond lengths on the square net are equal, a single nearest-neighbor magnetic coupling denoted by J on Figure 1a can describe the basic magnetic interactions. This spin model can be mapped onto a charge model known as the Hubbard Hamiltonian, $\mathcal{H} = -t\sum_{<i,j>,\sigma} c^{\dagger}_{i,\sigma}c_{j,\sigma} + U\sum_i n^{\dagger}_{i\uparrow}n_{i\downarrow}$, where the first term describes the hopping of electrons between neighboring sites with amplitude $t = 4J^2/U$ and the second term accounts for the Coulomb cost of double occupancy on a single site.[2,3] At half-filling, the Mott insulator orders antiferromagnetically, but upon doping, it undergoes a

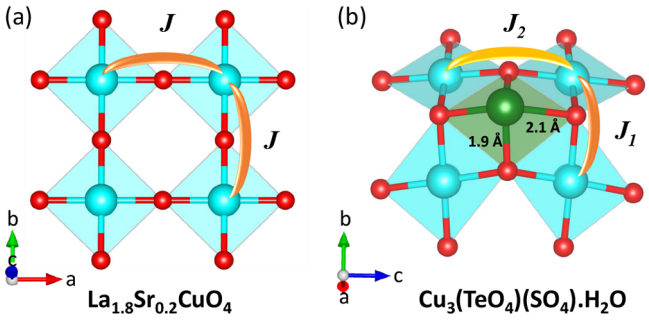

Figure 1. (a) Corner-sharing square-planar CuO_4 units with a Cu−O−Cu square net in a representative cuprate superconductor $La_{1.8}Sr_{0.2}CuO_4$ with a single J coupling. (b) Corrugated square net in $Cu_3(TeO_4)(SO_4)\cdot H_2O$ with two magnetic coupling constants $J_1 \geq J_2$.

Received: April 21, 2021

quantum phase transition into a superconducting state.[4,5] Despite several theoretical proposals, finding new Mott insulators with an electronic structure similar to that of the cuprates has become a major challenge in solid-state chemistry.[6]

Recently, it has been suggested that the copper tellurium oxides and hydroxides[7] could be a new playground for magnetism and superconductivity due to the half-filled bands from Cu^{2+} in such compounds as $CuTeO_4$, Sr_2CuTeO_6, $Cu_3TeO_6{\cdot}(H_2O)_2$, $MgCu_2TeO_6{\cdot}(H_2O)_6$, $K_2Cu_2(Te_2O_5)(TeO_3)_2{\cdot}(H_2O)_2$, and $Cu_6IO_3(OH)_{10}Cl$.[8−12] Although these materials could be magnetic insulators, none of them have a corner-shared square network of CuO_4 as shown in Figure 1a, which is necessary for the Hubbard model. Furthermore, most of these materials crystallize in the honeycomb, kagome, and maple-leaf structures,[7] except for $CuTeO_4$ and Sr_2CuTeO_6 that have a cubic unit cell, but without a 2D corner-shared square network.[8,9]

In this article, we present a new copper tellurite sulfate with the chemical formula $Cu_3(TeO_4)(SO_4){\cdot}H_2O$ whose quasi-2D lattice comprises a distorted square-planar network of Cu−O−Cu bonds as illustrated in Figure 1b. Each spin-1/2 Cu^{2+} ion interacts with its neighbors and creates a Mott insulating state with AFM ordering at T_N = 67 K, a description that fits the Hubbard model. Unlike the cuprates, a distinguishable feature of the phase is the buckled square network of Cu−O−Cu bonds due to the presence of a Te^{4+} ion in the center of every four corner-shared CuO_4 units (Figure 1b). As a result, the Te−O bond lengths vary between 1.9 and 2.1 Å leading to two AFM coupling constants denoted by J_1 and J_2 on Figure 1b. Thus, $Cu_3(TeO_4)(SO_4){\cdot}H_2O$ is an excellent candidate material for the extended Hubbard model with $J_1 \geq J_2$ due to the slightly shorter distance between Cu^{2+} ions across the J_1 superexhcange path compared to the J_2 path.[13] Our combined magnetization and heat capacity measurements reveal two magnetic transitions due to the two competing coupling constants. First, $Cu_3(TeO_4)(SO_4){\cdot}H_2O$ develops an AFM order at T_N = 67 K and then it undergoes a spin-canting transition at T^* = 12 K where the spins deviate from an ideal antiparallel alignment. Our findings in $Cu_3(TeO_4)(SO_4){\cdot}H_2O$ revive the search for new compounds with the potential for a Mott insulator ground state, extended Hubbard model, and possibly superconductivity.

■ EXPERIMENTAL SECTION

Crystal Growth. $Cu_3(TeO_4)(SO_4){\cdot}H_2O$ crystals were grown using a hydrothermal method. Starting materials $Cu(NO_3)_2{\cdot}2.5H_2O$ (5 g, 21.5 mmol), $Na_2S{\cdot}9H_2O$ (1.5 g, 6.2 mmol), Te powder (0.5 g, 3.9 mmol), and 4 mL of deionized water were loaded into a 10 mL Teflon liner (90% full) inside a steel autoclave and mixed with a glass stirring rod. The autoclave was kept at 220 °C for 250 h in a laboratory oven. The reaction had a high yield of approximately 1.5 g of $Cu_3(TeO_4)(SO_4){\cdot}H_2O$ crystals which we harvested after washing the solvent and byproducts with deionized water. The crystals were brittle, had a dark-green color, and grew with an acicular habit as shown in the inset of Figure S1 (Supporting Information). The reaction byproducts were $Cu_3(SO_4)(OH)_4$ (green powder) and $Cu_7(TeO_3)_2(SO_4)_2(OH)_6$ (turquoise crystals), with a ratio of Cu/Te/S = 3.5:1:1 close to the ratio in $Cu_3(TeO_4)(SO_4){\cdot}H_2O$.

X-ray Diffraction. A small single crystal with dimensions 0.03 × 0.03 × 0.09 mm^3 was selected and data were collected on a Bruker D8 Quest diffractometer equipped with an Incoatec microfocus source (IμS, Mo Kα radiation, λ = 0.71073 Å), and a PHOTON II CPAD area detector.[14] The collected frames were reduced using the Bruker SAINT software, and a multiscan absorption correction was applied using Bruker SADABS.[15] The initial structural model was developed with the intrinsic phasing feature of SHELXT[16] and a least-square refinement was performed using SHELXL2014.[17] We observed positional disorder of the solvent water molecules along the *b*-direction, which has been refined as disordered over a split site. The crystallographic information and refinement statistics are summarized in Table 1. The atomic coordinates and displacement parameters are presented in Table 2. Selected bond distances and Cu−Cu distances are provided in Table 3.

Table 1. Crystallographic Parameters and X-ray Refinement Statistics Summarized for a Single Crystal of $Cu_3(TeO_4)(SO_4){\cdot}H_2O$

space group	*Pnma* (no. 62)
a (Å)	15.974(2)
b (Å)	6.3468(8)
c (Å)	7.2563(14)
V ($Å^3$)	735.7(2)
Z	4
temperature (K)	298
θ range (deg)	2.6−30.6
μ (mm^{-1})	12.79
measured reflections	43 789
independent reflections	1220
R_{int}	0.100
h	−22 → 22
k	−9 → 9
l	−10 → 10
GoF	1.08
extinction coefficient	0.00330(17)
$R_1(F^2 > 2\sigma(F^2))^a$	0.014
$wR_2(F^2)^b$	0.034
$\Delta\rho_{max}$ (e $Å^{-3}$)	0.83
$\Delta\rho_{min}$ (e $Å^{-3}$)	−0.57

$^a R_1 = \sum||F_o| - |F_c||/\Sigma|F_o|$. $^b wR_2 = [\sum w(F_o^2 - F_c^2)^2/\sum w(F_o^2)^2]^{1/2}$.

Neutron Diffraction. A powder neutron diffraction experiment was performed on the BT-1 high-resolution powder diffractometer at the NIST Center for Neutron Research. Approximately 2 g of a $Cu_3(TeO_4)(SO_4){\cdot}H_2O$ powder sample was loaded in an aluminum canister, with 1 bar of helium exchange gas loaded at room temperature. The powder can was installed in a closed-cycle refrigerator with a base temperature of 4.6 K. We collected diffraction patterns using 60' collimation and the Ge(311) monochromator (λ = 2.079 Å) for *T* = 4.6, 25, and 100 K. All error bars shown in this work indicate one standard deviation. We could not resolve the magnetic Bragg peaks due to the large background from the incoherent scattering of neutrons by the hydrogen atoms; however, the analysis of neutron data has confirmed the X-ray structural refinement. Therefore, the neutron data are presented entirely in the Supporting Information.

Thermal Analysis. Thermogravimetric analysis (TGA) was performed using a TA Instruments Discovery SDT650 under a constant flow of N_2 (100 mL/min) and a heating rate of 1 °C/min to a maximum of 300 °C. The crushed crystals were placed in an alumina crucible without a lid for the experiment. The sample was held at 75 °C for 30 min before ramping to 300 °C to ensure thermal equilibrium and remove surface moisture.

Physical Measurements. The heat capacity was measured on a crystal cluster of mass 7.9 mg using a Quantum Design PPMS DynaCool with a relaxation-time technique. The flat surface of the crystal cluster was attached to the sample platform with Apiezon-N grease. DC magnetization measurements were performed using a Quantum Design MPMS3 on the same sample that we used for the heat capacity measurements. Energy-dispersive X-ray spectroscopy (EDX) was performed using an EDAX detector installed on a JEOL-

https://doi.org/10.1021/acs.inorgchem.1c01220
Inorg. Chem. XXXX, XXX, XXX−XXX

Table 2. Fractional Atomic Coordinates, Site Occupancies, and Equivalent Isotropic Displacement Parameters (U_{eq}) Are Listed for Each Wyckoff Site in the Structure of $Cu_3(TeO_4)(SO_4)\cdot H_2O$[a]

atom	site	x	y	z	U_{eq} (Å^2)	occ.
Te1	4c	0.13721(2)	1/4	0.64673(2)	0.00792(6)	1
Cu1	8d	0.25156(2)	0.50293(3)	0.88327(3)	0.00910(7)	1
Cu2	4c	0.40689(2)	3/4	0.67012(5)	0.01054(8)	1
S1	4c	0.57556(4)	3/4	0.41099(9)	0.00811(13)	1
O1	4c	0.32502(12)	3/4	0.8654(2)	0.0078(4)	1
O2	4c	0.18265(12)	1/4	0.9060(2)	0.0084(4)	1
O3	8d	0.20930(10)	0.4893(2)	0.63332(17)	0.0114(3)	1
O4	8d	0.59172(10)	0.5649(2)	0.2921(2)	0.0161(3)	1
O5	4c	0.48693(12)	3/4	0.4662(3)	0.0144(4)	1
O6	4c	0.63037(13)	3/4	0.5712(3)	0.0187(4)	1
O7	4c	0.5340(2)	0.717(2)	0.8939(4)	0.032(3)	0.5
H1	8d	0.551(3)	0.675(8)	0.997(4)	0.048	0.5
H2	8d	0.579(2)	0.756(19)	0.839(6)	0.048	0.5

[a]The atomic displacement parameters of H1 and H2 were refined isotropically whereas all the other atoms were refined anisotropically.

Table 3. Selected Bond Distances and Cu−Cu Distances

Te1−O1	2.1285(18)
Te1−O2	2.0166(18)
Te1−O3 (×2)	1.9087(14)
Cu1−O1	1.9628(12)
Cu1−O2	1.9535(11)
Cu1−O3	1.9371(13)
Cu1−O3	1.9198(13)
Cu2−O1	1.9286(18)
Cu2−O4 (×2)	2.0176(14)
Cu2−O5	1.955(2)
S1−O4 (×2)	1.4801(14)
S1−O5	1.471(2)
S1−O6	1.455(2)
Cu1−Cu1 (b direction)	3.1362(6)
Cu1−Cu1 (c direction)	3.6287(8)
Cu1−Cu1(diagonal)	4.8204(6)
Cu1−Cu2 (short)	3.3178(5)
Cu1−Cu2 (long)	3.6491(6)
Cu2−Cu2 (b direction)	6.3468(9)
Cu2−Cu2 (c direction)	7.256(2)
Cu2−Cu2 (diagonal)	5.0015(7)

7900F field-emission electron microscope (FESEM). The spectra were obtained from the fresh surface of a crystal and confirmed the chemical formula of the title compound (Supporting Information, Figure S1).

■ RESULTS AND DISCUSSION

Synthesis. Our hydrothermal synthesis of $Cu_3(TeO_4)(SO_4)\cdot H_2O$ can be described as a redox reaction where the element Te and anion S^{2-} are oxidized to cations Te^{4+} and S^{6+}. The possibility of O_2 as the oxidant is ruled out because the reactants are sealed in the autoclave and there is too little remaining O_2 to oxidize Te and Na_2S. Candidate reduction reactions include $2H^+ \rightarrow H_2$, $Cu^{2+} \rightarrow Cu^+$, and $NO_3^- \rightarrow NO_2^-$. In the case of $2H^+ \rightarrow H_2$, the reaction would produce an enormous gas pressure (~10^3 bar) and rupture the blow-off valve on the autoclave. Since we do not see evidence of such damage, we rule out this possibility. If Cu^{2+} is reduced to Cu^+, then the chemical equation must be $15Cu^{2+}(NO_3)_2 + Na_2S + Te + 9H_2O \rightarrow Cu_3^{2+}(TeO_4)(SO_4)\cdot H_2O + 2NaNO_3 + 16HNO_3 + 12Cu^+NO_3$. We also rule out this possibility on the basis of three observations: (i) the product contains Cu^+, which is not stable in an oxidizing environment; (ii) the reaction requires a large amount of the $Cu(NO_3)_2$ reagent and produces only a small amount of $Cu_3(TeO_4)(SO_4)\cdot H_2O$, which is inconsistent with the observed high yield of the reaction; and (iii) the reaction completely fails if $Cu(NO_3)_2\cdot 2.5H_2O$ is replaced with $CuSO_4\cdot 5H_2O$ as the starting material, which means that the reduction of NO_3^- to NO_2^- is crucial to achieving the title compound. Thus, the redox reaction can be described only as

$$3Cu(NO_3)_2 + Na_2S + Te + 3H_2O \rightarrow Cu_3(TeO_4)(SO_4)\cdot H_2O + 2NaNO_2 + 4HNO_2 \quad (1)$$

which is consistent with both the high yield of the reaction and the crucial role of $Cu(NO_3)_2$ in the synthesis.

Structural Analysis. $Cu_3(TeO_4)(SO_4)\cdot H_2O$ crystallizes in the orthorhombic space group *Pnma* with two Cu, one Te, one S, and seven O sites. Figure 2a shows that each corrugated plane in the quasi-2D structure of $Cu_3(TeO_4)(SO_4)\cdot H_2O$ is made of corner-sharing CuO_4 squares (Cu1 site) along both the b and c directions as well as edge-sharing CuO_4 squares and TeO_4 pyramids along the ⟨011⟩ directions. Figure 2b shows that the corrugated layers are linked by slabs of interconnected corner-sharing CuO_4 (Cu2 site) and SO_4 units. The orientation of these slabs alternates between [10$\bar{1}$] and [101]. The H_2O molecules are inserted between the slabs and diffused along the b axis.

Figure 2c shows the local environment of distorted square-planar CuO_4 with bond lengths ranging from 1.9198(13) to 2.0176(14) Å, in agreement with Cu−O bond lengths of 1.9 to 2.1 Å in Cu^{2+} compounds $Cu_7TeO_4(SO_4)_5\cdot KCl$[18] and $Cu_7(TeO_3)_2(SO_4)_2(OH)_6$.[19] The O−Cu−O bond angles in the CuO_4 units range from 81.15(7) to 100.5(6)°, comparable to the bond angles of 79 to 95° in $Cu_7TeO_4(SO_4)_5\cdot KCl$[18] and 75.0(2) to 98.3(2)° in $Cu_2Te_3O_8$.[20] We present a detailed analysis of the bond valence sum (BVS) using the local coordination in the Supporting Information (Table S1). A summary of those results is presented in Table 4. The bond valence around the Cu1 site sums to 1.922, confirming a 2+ state. However, the bond valence around the Cu2 site sums to 1.480 assuming a 1+ state and 1.746 assuming a 2+ state, indicating a mixed valence of Cu^{2+}/Cu^+ for the Cu2 site.

The Te−O bond distances and the coordination environment for Te are consistent with a Te(IV) oxidation state and

https://doi.org/10.1021/acs.inorgchem.1c01220
Inorg. Chem. XXXX, XXX, XXX−XXX

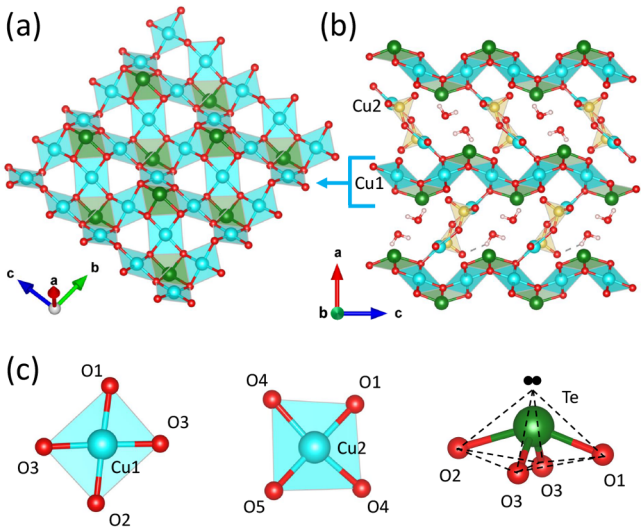

Figure 2. (a) Corrugated *bc* planes in the crystal structure of $Cu_3(TeO_4)(SO_4)\cdot H_2O$ comprise corner-sharing CuO_4 squares and edge-sharing CuO_4−TeO_4 units. The Cu, Te, S, and O atoms appear as blue, green, yellow, and red spheres, respectively. (b) *b*-axis view shows the corrugated layers linked by corner-sharing CuO_4−SO_4 slabs with alternating directions. The H_2O molecules reside in the channels parallel to the *b* axis. (c) Local distorted square-planar coordination around Cu1 and Cu2 sites and the trigonal bipyramidal coordination around Te^{4+}. The repulsion between the lone pair and bonding electrons within each TeO_4 unit leads to the corrugated layer structure.

Table 4. Bond Valence Sum Values for the Cation Sites in $Cu_3(TeO_4)(SO_4)\cdot H_2O$

atomic site	BVS	expected value
Cu1	1.922	+2
Cu2	1.746/1.480	+2/+1
Te	3.766	+4
S	6.038	+6

comparable to the Te−O bond length range of 1.9 to 2.1 Å in trigonal bipyramidal TeO_4 in α-TeO_2.[21] The trigonal bipyramid coordination for Te is rarely observed in copper tellurium sulfates and, to the best of our knowledge, was reported only as a tetragonal pyramid in $Cu_7TeO_4(SO_4)_5\cdot KCl$.[18] The average Te−O bond lengths of the title compound range from 1.9087(14) to 2.1285(18) Å, comparable to those of several other copper tellurium oxides such as $Cu_7TeO_4(SO_4)_5\cdot KCl$, $Ba_2Cu_2Te_2P_2O_{13}$,[22] $Cu_2Te_3O_8$,[20] $Nb_2Te_4O_{13}$,[23] and $BaCuTeO_3TeO_4$.[24] The O_{ax}−Te−O_{eq} (axial and equatorial oxygens) bond angles in $Cu_3(TeO_4)(SO_4)\cdot H_2O$ of 80.23(5) and 77.29(5)° are comparable to the pairs of tetragonal pyramidal bond angles of 90.5 and 87.9° in $Cu_7TeO_4(SO_4)_5\cdot KCl$.[18] The reduction in the bond angle in the title compound can be due to the repulsion between the lone pair and the bonding electrons in each TeO_4 unit within the corrugated layer (Figure 2c).

THERMAL ANALYSIS

Figure 3 shows the change in the mass of $Cu_3(TeO_4)(SO_4)\cdot H_2O$ with increasing temperature of up to 300 °C under a nitrogen atmosphere. A weight loss of 3.4(1) wt % is observed, which is in agreement with the expected 3.6 wt % corresponding to one H_2O molecule per formula unit. We

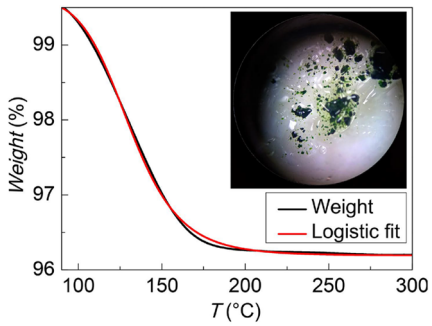

Figure 3. TGA curve (black) of $Cu_3(TeO_4)(SO_4)\cdot H_2O$ and a logistic fit (red) with good quality (R^2 > 0.998). (Inset) Crystals after dehydration.

fitted the TGA data using a logistic function, $p_w = B + \frac{A-B}{1+\left(\frac{T}{T_0}\right)^p}$, where A and B are the initial and final weight percentages in the dehydration experiment, T_0 is the temperature at which half of the water has been removed, and p determines the rate of dehydration. We determined the midpoint of the dehydration to be T_0 = 131(1) °C, and the parameter p was 8.620(3). The 3.4(1) % weight loss was found by subtracting the fit parameter A = 99.6327(4)% from B = 96.1918(1)%. Interestingly, the sample changed from black to transparent dark green during the experiment, while the crystal structure stayed intact. This could indicate a change in the mixed oxidations state of Cu2 in favor of Cu^{2+}. The most likely scenario is that Cu^+ ions between the layers (Cu2 site) are conjugated with hydronium ions (H_3O^+) to maintain charge neutrality. Upon dehydration, however, most of the Cu^+ will turn into Cu^{2+}.

MAGNETIC PROPERTIES

Figure 4a displays the temperature dependence of the magnetic susceptibility $\chi(T)$ in $Cu_3(TeO_4)(SO_4)\cdot H_2O$ under an external field of 0.1 T. A sharp peak at T_N = 67(1) K suggests an AFM phase transition. The inverse susceptibility is fitted to the Curie−Weiss expression $\chi = C/(T-\Theta_W) + \chi_0$ using the data between 250 and 400 K. From this fit, we obtain a negative Weiss temperature Θ_W = −137 K, confirming AFM correlations above T_N. The effective moment extracted from the Curie−Weiss fit is $1.2\mu_B$/Cu, which is 71% of the expected value ($1.73\mu_B$/Cu) for Cu^{2+} (g = 2, S = 1/2). On the basis of the BVS analysis mentioned earlier, the mixed valence of the Cu2 site (interlayer coppers) is responsible for the reduced moment. Since the occupancy of the Cu1 site (8*d*) is twice that of the Cu2 site (4*c*), the reduced moment corresponds to 88% Cu^+ in the Cu2 site. Thus, most of the interlayer copper ions are nonmagnetic, which makes the analogy between $Cu_3(TeO_4)(SO_4)\cdot H_2O$ and superconducting cuprates more highly justified. In cuprates, the interlayer ions are nonmagnetic (e.g., La^{3+} and Sr^{2+}). On the basis of the Curie−Weiss fit analysis and the obtained magnetic moment, the exact formula can be represented as $Cu_{3-x}{}^{2+}Cu_x{}^{+}(TeO_4)^{4-}(SO_4)^{2-}(H_2O)_{1-x}(H_3O^+)_x$, where $x \approx 0.88$. The hydronium ion (H_3O^+) is introduced to balance the charge, as we mentioned earlier. Nevertheless, we use the formula $Cu_3(TeO_4)(SO_4)\cdot H_2O$ for a simple presentation.

The heat capacity data shown in Figure 4b are consistent with the magnetic susceptibility data. A peak at 67 K in the right inset of Figure 4b is clearly discernible even with the

https://doi.org/10.1021/acs.inorgchem.1c01220
Inorg. Chem. XXXX, XXX, XXX−XXX

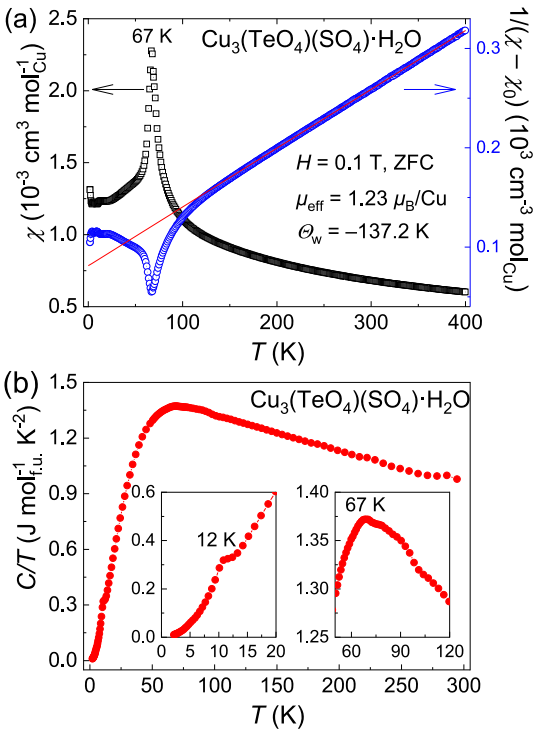

Figure 4. (a) Temperature dependence of the magnetic susceptibility (left axis) and inverse susceptibility (right axis) in $Cu_3(TeO_4)(SO_4)\cdot H_2O$ under a magnetic field of 0.1 T in zero-field-cooling (ZFC) mode. The red solid line is a Curie−Weiss fit to the data between 250 and 400 K. Due to the acicular habit of crystals, the field direction is not specified in Figures 4, 5, and 6. (b) C/T under zero field as a function of temperature. The insets magnify the transitions at T^* = 12 K (left) and T_N = 67 K (right).

dominant phonon background in the high-temperature regime. It confirms the AFM transition observed in the susceptibility data at 67 K in Figure 4a. In addition, a kink is observed in the heat capacity at T^* = 12 K, which is magnified in the left inset of Figure 4b. As explained below, we attribute this feature to a spin-canting transition using the field dependence of magnetization.

To examine the phase transition at T^* = 12 K, we studied the field dependence of the magnetic susceptibility under zero-field-cooled (ZFC) and field-cooled (FC) conditions (Figure 5). Under a small magnetic field (less than 1 T), the AFM peak is accompanied by a splitting between the ZFC and FC data in Figure 5a, suggesting a small ferromagnetic component in addition to the obvious AFM order. Such behavior can result from a small deviation from the strictly antiparallel arrangement of spins in a canted AFM.[25] With increasing field to 2 T, the ZFC/FC splitting disappears below T_N = 67 K but remains visible below T^* = 12 K. This trend becomes even clearer at 3 T, where two peaks are observed: one at 67 K without the ZFC/FC splitting and another at 12 K with the splitting. The splitting below 12 K survives up to 5 T as shown in Figure 5d. We interpret this behavior as a Néel-type transition at T_N = 67 K, followed by a spin-canting transition below T^* = 12 K.

Further evidence of a spin-canting transition at 12 K comes from the evolution of isothermal magnetization loops in Figure 6. At $T > T_N$, the $M(H)$ curves are linear as seen in Figure 6a,b. With decreasing temperature below T_N = 67 K, a small step-like increase is observed in the $M(H)$ curves at a critical magnetic field which is moderately suppressed from H_c = 3 to

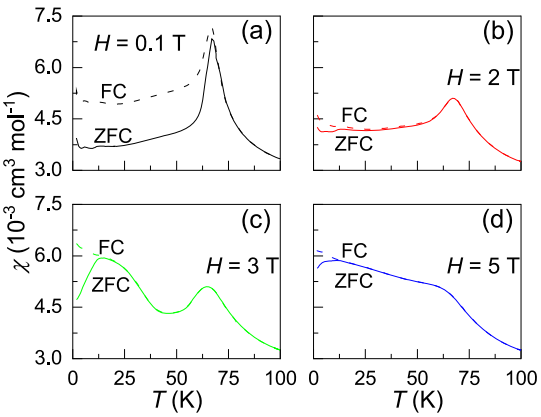

Figure 5. Temperature dependence of the magnetic susceptibility below 100 K under different fields at (a) 0.1 T, (b) 2 T, (c) 3 T, and (d) 5 T. The solid and dashed lines represent the ZFC and FC conditions, respectively.

2.3 T as the temperature is decreased from 50 to 15 K. The step-like transition could be a mild spin-flop in the AFM ordered Cu^{2+} moments. A similar phenomenon is reported in Ni_3TeO_6,[26] another layered material containing three Ni sites. With further decreasing temperature below T^* = 12 K, a hysteresis loop opens in the $M(H)$ curves, confirming an FM component in the magnetic order as expected from a spin-canting transition.[27] Note that the spin-canting transition and the resulting FM component are well justified by the presence of two competing coupling constants J_1 and J_2 (Figure 1b).

■ CONCLUSIONS

The salient features of $Cu_3(TeO_4)(SO_4)\cdot H_2O$ can be summarized as follows. It is a layered material with spin-1/2 Cu^{2+} ions within the layers and mixed valence Cu^{2+}/Cu^{+} between the layers. The layers are made of corner-sharing CuO_4 square-planar units in the *bc* plane, which are corrugated due to edge-sharing between the CuO_4 and TeO_4 units. These features are reminiscent of the high-T_c cuprate superconductors,[28] but unlike the cuprates, the layers are corrugated in $Cu_3(TeO_4)(SO_4)\cdot H_2O$. Despite tremendous effort by materials experts, it has been difficult to identify new families of compounds with such structural motifs and a Mott insulating AFM ground state. In this regard, $Cu_3(TeO_4)(SO_4)\cdot H_2O$ is a promising candidate material which is also available in single-crystal form. The AFM transition temperature of 67 K and the half-filling of Cu^{2+} confirm a Mott insulating ground state. The spin-canting transition at 12 K requires at least two different superexchange couplings J_1 and J_2, consistent with the different bond lengths in Figure 1b. A J_1/J_2 magnetic model has been theoretically proposed to harbor both superconductivity and spin liquid behavior in cuprates.[29,30] However, the largest J_1/J_2 ratio in cuprates is around 0.5, since J_2 is a next-nearest-neighbor interaction.[29−31] Remarkably, $Cu_3(TeO_4)(SO_4)\cdot H_2O$ provides access to a J_1/J_2 ratio close to 1 due to the small difference between the J_1 and J_2 superexchange paths (Figure 1b). Evidence of a mild magnetic frustration, due to the competition between J_1 and J_2, can be observed in Figure 4a, where the Weiss temperature (Θ_W = −137 K) is twice as large as the Néel temperature (T_N = 67 K). Future research directions from here would be to find whether T_N can be suppressed under pressure, leading to a spin liquid ground state, or if it can be suppressed by doping (e.g.,

https://doi.org/10.1021/acs.inorgchem.1c01220
Inorg. Chem. XXXX, XXX, XXX−XXX

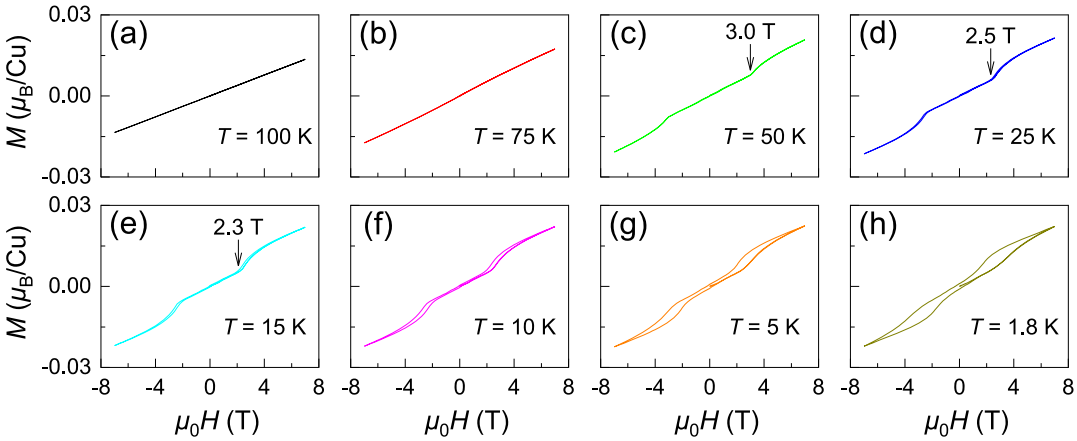

Figure 6. Isothermal magnetization loops in $Cu_3(TeO_4)(SO_4)\cdot H_2O$ at several temperatures (a, b) above T_N, (c−e) between T^* = 12 K and T_N = 67 K, and (f−h) below T^*.

replacing the interlayer Cu atoms with Ag, Zn, and Ca) to induce superconductivity. It will also be instructive to synthesize a deuterated version of $Cu_3(TeO_4)(SO_4)\cdot H_2O$ to solve the magnetic structure using neutron diffraction. The intricate chemistry of tellurite-sulfate systems and the versatility of the hydrothermal method are likely to produce more such materials in the future.

■ ASSOCIATED CONTENT

Supporting Information

The Supporting Information is available free of charge at https://pubs.acs.org/doi/10.1021/acs.inorgchem.1c01220.

Energy-dispersive X-ray spectroscopy; neutron diffraction; bond valence sum calculations; and bond valence sum for $Cu_3(TeO_4)(SO_4)H_2O$ (PDF)

Accession Codes

CCDC 2076676 contains the supplementary crystallographic data for this paper. These data can be obtained free of charge via www.ccdc.cam.ac.uk/data_request/cif, or by emailing data_request@ccdc.cam.ac.uk, or by contacting The Cambridge Crystallographic Data Centre, 12 Union Road, Cambridge CB2 1EZ, UK; fax: +44 1223 336033.

■ AUTHOR INFORMATION

Corresponding Authors

Zhi-Cheng Wang − *Department of Physics, Boston College, Chestnut Hill, Massachusetts 02467, United States;* orcid.org/0000-0003-0100-3900; Phone: (617) 552-2127; Email: zhicheng.wang@bc.edu

Fazel Tafti − *Department of Physics, Boston College, Chestnut Hill, Massachusetts 02467, United States;* orcid.org/0000-0002-5723-4604; Phone: (617) 552-2127; Email: fazel.tafti@bc.edu

Authors

Kulatheepan Thanabalasingam − *Department of Chemistry and Biochemistry, University of Texas at Dallas, Richardson, Texas 75080, United States*

Jan P. Scheifers − *Department of Chemistry and Biochemistry, University of Texas at Dallas, Richardson, Texas 75080, United States*

Alenna Streeter − *Department of Physics, Boston College, Chestnut Hill, Massachusetts 02467, United States*

Gregory T. McCandless − *Department of Chemistry and Biochemistry, University of Texas at Dallas, Richardson, Texas 75080, United States*

Jonathan Gaudet − *Department of Materials Science and Engineering, Maryland University, College Park, Maryland 20942-2115, United States; NIST Center for Neutron Research, National Institute of Standards and Technology, Gaithersburg, Maryland 20899-6102, United States*

Craig M. Brown − *NIST Center for Neutron Research, National Institute of Standards and Technology, Gaithersburg, Maryland 20899-6102, United States;* orcid.org/0000-0002-9637-9355

Carlo U. Segre − *Department of Physics & CSRRI, Illinois Institute of Technology, Chicago, Illinois 60616, United States;* orcid.org/0000-0001-7664-1574

Julia Y. Chan − *Department of Chemistry and Biochemistry, University of Texas at Dallas, Richardson, Texas 75080, United States;* orcid.org/0000-0003-4434-2160

Complete contact information is available at: https://pubs.acs.org/10.1021/acs.inorgchem.1c01220

Notes

The authors declare no competing financial interest.

■ ACKNOWLEDGMENTS

The work at Boston College was funded by the National Science Foundation under award number DMR-1708929. The work at UT Dallas was funded by the National Science Foundation under award number DMR-1700030. We acknowledge the support of the National Institute of Standards and Technology in providing the neutron research facilities used in this work. The identification of any commercial product or trade name does not imply endorsement or recommendation by the National Institute of Standards and Technology.

■ REFERENCES

(1) Phillips, P. W.; Yeo, L.; Huang, E. W. Exact theory for superconductivity in a doped Mott insulator. *Nat. Phys.* **2020**, *16*, 1175−1180.

(2) Anderson, P. W. Twenty-five years of high-temperature superconductivity − A personal review. *J. Phys.: Conf. Ser.* **2013**, *449*, 012001.

(3) Foley, A.; Verret, S.; Tremblay, A.-M. S.; Sénéchal, D. Coexistence of superconductivity and antiferromagnetism in the

Hubbard model for cuprates. *Phys. Rev. B: Condens. Matter Mater. Phys.* **2019**, *99*, 184510.
(4) Lee, P. A.; Nagaosa, N.; Wen, X.-G. Doping a Mott insulator: Physics of high-temperature superconductivity. *Rev. Mod. Phys.* **2006**, *78*, 17−85.
(5) Jiang, H.-C.; Devereaux, T. P. Superconductivity in the doped Hubbard model and its interplay with next-nearest hopping t. *Science* **2019**, *365*, 1424−1428.
(6) Baskaran, G. Five-fold way to new high T_c superconductors. *Pramana* **2009**, *73*, 61−112.
(7) Norman, M. R. Copper tellurium oxides − A playground for magnetism. *J. Magn. Magn. Mater.* **2018**, *452*, 507−511.
(8) Falck, L.; Lindqvist, O.; Mark, W.; Philippot, E.; Moret, J. The crystal structure of $CuTeO_4$. *Acta Crystallogr., Sect. B: Struct. Crystallogr. Cryst. Chem.* **1978**, *34*, 1450−1453.
(9) Iwanaga, D.; Inaguma, Y.; Itoh, M. Crystal Structure and Magnetic Properties of B-Site Ordered Perovskite-type Oxides $A_2CuB'O_6$ (A = Ba, Sr; B'=W, Te). *J. Solid State Chem.* **1999**, *147*, 291−295.
(10) Grice, J.; Groat, L.; Roberts, A. Jensenite, a cupric tellurate framework structure with two coordinations of copper. *Can. Mineral.* **1996**, *34*, 55−59.
(11) Margison, S. M.; Grice, J. D.; Groat, L. A. The crystal structure of leisingite, $(Cu^{2+},Mg,Zn)_2$ $(Mg,Fe)Te^{6+}O_6.6H_2O$. *Can. Mineral.* **1997**, *35*, 759−763.
(12) Mills, S. J.; Kampf, A. R.; Christy, A. G.; Housley, R. M.; Rossman, G. R.; Reynolds, R. E.; Marty, J. Bluebellite and mojaveite, two new minerals from the central Mojave Desert, California, USA. *Mineral. Mag.* **2014**, *78*, 1325−1340.
(13) Tocchio, L. F.; Montorsi, A.; Becca, F. Magnetic and spin-liquid phases in the frustrated $t-t'$ Hubbard model on the triangular lattice. *Phys. Rev. B: Condens. Matter Mater. Phys.* **2020**, *102*, 115150.
(14) Certain commercial equipment, instruments, or materials are identified in this document. Such identification does not imply recommendation or endorsement by the National Institute of Standards and Technology, nor does it imply that the products identified are necessarily the best available for the purpose.
(15) Krause, L.; Herbst-Irmer, R.; Sheldrick, G. M.; Stalke, D. Comparison of silver and molybdenum microfocus X-ray sources for single-crystal structure determination. *J. Appl. Crystallogr.* **2015**, *48*, 3−10.
(16) Sheldrick, G. M. SHELXT - Integrated space-group and crystal-structure determination. *Acta Crystallogr., Sect. A: Found. Adv.* **2015**, *71*, 3−8.
(17) Sheldrick, G. M. Crystal structure refinement with SHELXL. *Acta Crystallogr., Sect. C: Struct. Chem.* **2015**, *71*, 3−8.
(18) Pertlik, F.; Zemann, J. The crystal structure of nabokoite, $Cu_7TeO_4(SO_4)_5.KCl$: The first example of a $Te(IV)O_4$ pyramid with exactly tetragonal symmetry. *Mineral. Petrol.* **1988**, *38*, 291−298.
(19) Guo, W.-B.; Tang, Y.-Y.; Wang, J.; He, Z. Layered $Cu_7(TeO_3)_2(SO_4)_2(OH)_6$ with Diluted Kagomé Net Containing Frustrated Corner-Sharing Triangles. *Inorg. Chem.* **2017**, *56*, 1830−1834.
(20) Feger, C. R.; Schimek, G. L.; Kolis, J. W. Hydrothermal Synthesis and Characterization of $M_2Te_3O_8$ (M = Mn, Co, Ni, Cu, Zn): A Series of Compounds with the Spiroffite Structure. *J. Solid State Chem.* **1999**, *143*, 246−253.
(21) Lindqvist, O. Refinement of structure of α-TeO_2. *Acta Chem. Scand.* **1968**, *22*, 977.
(22) Xia, M.; Shen, S.; Lu, J.; Sun, Y.; Li, R. $Ba_2Cu_2Te_2P_2O_{13}$: A new telluro-phosphate with S = 1/2 Heisenberg chain. *J. Solid State Chem.* **2015**, *230*, 75−79.
(23) Jiang, N.; Spence, J. C. H. Intermediate-range structure of tellurite glasses from near-edge absorption spectra. *Phys. Rev. B: Condens. Matter Mater. Phys.* **2004**, *70*, 184113.
(24) Sedello, O.; Müller-Buschbaum, H. Synthese und Kristallstruktur des Barium -Kupfer-Tellurit-Tellurats $BaCuTeO_3TeO_4$/ Synthesis and Crystal Structure of the Barium Copper Tellurite-Tellurate $BaCuTeO_3TeO_4$. *Z. Naturforsch., B: J. Chem. Sci.* **1996**, *51*, 465−468.
(25) Cao, C.; Liu, S.-J.; Yao, S.-L.; Zheng, T.-F.; Chen, Y.-Q.; Chen, J.-L.; Wen, H.-R. Spin-Canted Antiferromagnetic Ordering in Transition Metal−Organic Frameworks Based on Tetranuclear Clusters with Mixed V- and Y-Shaped Ligands. *Cryst. Growth Des.* **2017**, *17*, 4757−4765.
(26) Oh, Y. S.; Artyukhin, S.; Yang, J. J.; Zapf, V.; Kim, J. W.; Vanderbilt, D.; Cheong, S.-W. Non-hysteretic colossal magnetoelectricity in a collinear antiferromagnet. *Nat. Commun.* **2014**, *5*, 3201.
(27) Li, D.; Han, Z.; Zheng, J. G.; Wang, X. L.; Geng, D. Y.; Li, J.; Zhang, Z. D. Spin canting and spin-flop transition in antiferromagnetic Cr_2O_3 nanocrystals. *J. Appl. Phys.* **2009**, *106*, 053913.
(28) Guo, Y.; Langlois, J.-M.; Goddard, W. A. Electronic Structure and Valence-Bond Band Structure of Cuprate Superconducting Materials. *Science* **1988**, *239*, 896−899.
(29) Yu, J.-F.; Kao, Y.-J. Spin-1/2 J_1-J_2 Heisenberg antiferromagnet on a square lattice: A plaquette renormalized tensor network study. *Phys. Rev. B: Condens. Matter Mater. Phys.* **2012**, *85*, 094407.
(30) Yu, S.-L.; Wang, W.; Dong, Z.-Y.; Yao, Z.-J.; Li, J.-X. Deconfinement of spinons in frustrated spin systems: Spectral perspective. *Phys. Rev. B: Condens. Matter Mater. Phys.* **2018**, *98*, 134410.
(31) Tanaka, K.; Yoshida, T.; Fujimori, A.; Lu, D. H.; Shen, Z.-X.; Zhou, X.-J.; Eisaki, H.; Hussain, Z.; Uchida, S.; Aiura, Y.; Ono, K.; Sugaya, T.; Mizuno, T.; Terasaki, I. Effects of next-nearest-neighbor hopping t' on the electronic structure of cuprate superconductors. *Phys. Rev. B: Condens. Matter Mater. Phys.* **2004**, *70*, 092503.

https://doi.org/10.1021/acs.inorgchem.1c01220
Inorg. Chem. XXXX, XXX, XXX−XXX